Available online at www.sciencedirect.com
ScienceDirect
Materials Research Bulletin 43 (2008) 3433–3440
Materials Research Bulletin
www.elsevier.com/locate/matresbu

Synthesis and optical properties of hierarchical pure ZnO nanostructures

D.H. Fan, Y.F. Zhu, W.Z. Shen *, J.J. Lu

Laboratory of Condensed Matter Spectroscopy and Opto-Electronic Physics, Department of Physics, Shanghai Jiao Tong University, 1954 Hua Shan Road, Shanghai 200030, PR China

Received 27 August 2007; received in revised form 10 January 2008; accepted 1 February 2008
Available online 9 February 2008

Abstract

We report the catalyst-free synthesis of hierarchical pure ZnO nanostructures with 6-fold structural symmetry by two-step thermal evaporation process. At the first step, the hexagonal-shaped nanowires consisting of a great deal of Zn and little oxide were prepared via the layer-by-layer growth mechanism; and at the second step, hierarchical pure ZnO nanostructures were synthesized by evaporating the Zn source on the basis of the step-one made substrate. Scanning electron microscopy, transmission electron microscope images, and the corresponding selected area electron diffraction pattern have been utilized to reveal the screw dislocation growth mechanism, through which the single crystal ZnO nanorods are epitaxially grown from the side-wall of central axial nanowires. Raman and photoluminescence spectra further indicate that, for the hierarchical ZnO nanostructures, the ultraviolet peak is related to the free exciton recombination, while the oxygen vacancies and high surface-to-volume ratio are responsible for the strong green peak emission.

Keywords: A. Nanostructures; B. Vapor deposition; C. Electron microscopy; C. X-ray diffraction; D. Optical properties

1. Introduction

Zinc oxide (ZnO) is an excellent candidate for the fabrication of optoelectronic and electronic device due to the high chemical stability, wide band gap of 3.37 eV and large exciton binding energy (60 meV) at room temperature. Especially, one-dimensional (1D) or quasi-1D ZnO nanostructures have attracted much attention owing to their unique and fascinating properties. It has been demonstrated that they can be applied potentially in the nanoresonators, nanolasings, photodetectors, photonic crystals, optical modulator waveguides, field emitters, light-emitting diodes, gas sensors, solar cells [1–9], and so on. By far, many kinds of 1D ZnO nanostructures have been prepared, such as nanobelts, nanorings, nanowires, nanoprisms, nanobridges, nanonails, nanopropellers, nanowhiskers, nanotubes, and nanopores [10–18].

Multifunctional devices communicating with many receivers would demand higher integrated nanostructures. However, the monotonic line nanostructures, including nanowire, nanorod, nanobelt, and so on, restrict themselves from being applied in the advanced system because of the simple shape and relative low integration degree. Recently,

* Corresponding author. Fax: +86 21 54743242.
E-mail address: wzshen@sjtu.edu.cn (W.Z. Shen).

0025-5408/$ – see front matter © 2008 Elsevier Ltd. All rights reserved.
doi:10.1016/j.materresbull.2008.02.001

many efforts have been made to prepare hierarchical nanostructures with high surface area, integration degree, and structural integrity [14,15,19–21]. Gao et al., [19] have prepared the rotor-like ZnO nanostructure by hydrothermal method. The hierarchical ZnO nanostructures with 6-, 4-, and 2-fold structural symmetry have been synthesized on In_2O_3 core nanowire by heating the intermixture of ZnO, In_2O_3 and graphite powders at ~1000 °C [21]. During their growth, the complicated synthetic procedures or the introduction of impurities are detrimental to the properties of the device. Exploring simple, cheap, catalyst-free and low-temperature methods of synthesizing hierarchical ZnO nanostructures still remains a challenge.

In this paper, we demonstrate a simple two-step thermal evaporation process to synthesize the hierarchical pure ZnO nanostructures of 6-fold structural symmetry without any metal catalyst. Our present method is to use the one-step-prepared samples as the substrate, and then synthesize the hierarchical nanostructures on that substrate. The new growth scheme is different from the former reported ones that only changed the heating temperature or gas pressure [15,22]. Compared with other methods, the present technique is simple, cheap and does not need the high temperature growth environment. In addition, only metallic zinc powder and silicon substrate are used without any additives. The selected area electron diffraction (SAED) analyses of nanorods reveal that single crystal ZnO nanorods epitaxially grow from the side-wall of central axial ZnO nanowires. The as-deposited samples exhibit strong green emission being related with the oxygen vacancies, which implies that this nanostructure has high electrical conductivity, and may be applied in electron nanoconductors in multichannel optoelectronic devices [22]. Present method also provides the possibility of a general approach to prepare hierarchical nanostructures made from other materials at relative low temperature.

2. Experimental details

The hierarchical ZnO nanostructures were synthesized in a horizontal tube furnace system by a two-step thermal vapor deposition process. In the first step, pure zinc powder (99.99%) of 0.6 g was placed in an alumina boat locating at the center of a horizontal quartz tube. N-type Si wafer cleaned by sonication in ethanol and acetone was used as the substrate and placed along the downstream position of carrier gas. The quartz tube was evacuated to ~2.0 Pa using a mechanical rotary pump to remove the residual oxygen before heating. When the source material was heated to 500 °C at a rate of 10 °C/min, pure (99.9%) argon and oxygen were used as the carrier gas and introduced from one end of the quartz tube at a flow rate of 300 and 80 standard cubic centimeters per minute (sccm), respectively. The duration at 500 °C of Zn source, the distance between Zn source and substrate, the work pressure, and the measured substrate temperature were 60 min, 34 cm, 180 Pa and about 200 °C, respectively. After heating, the tube was cooled naturally to room temperature under the above-mentioned atmosphere, and gray products were found covering the silicon substrate.

In the following step, the one-step-prepared samples were used as the substrates to prepare the hierarchical pure ZnO nanostructures. They were also placed along the downstream side of the carrier gas. Argon and oxygen were still used as the carrier gas at a flow rate of 260 and 90 sccm, respectively. In the experiment, the Zn source at the centre of horizontal tube furnace was still heated to 500 °C with the duration time of 80 min. The distance between Zn source and substrate, the work pressure, and the measured substrate temperature were 2 cm, ~180 Pa and about 500 °C, respectively. After the reaction, the quartz tube was again cooled naturally to room temperature and the color of sample surface became gray-white from gray. The post-annealing of two-step-prepared samples was carried out in the pure oxygen atmosphere for 1 h at 600 °C. After annealing, the samples were naturally cooled down.

The morphology and structure of the samples were characterized using the field-emission scanning electron microscopy (FESEM) (Philips XL30FEG), the high resolution transmission electron microscope (HRTEM) (JEOL JEM-2100F), and X-ray diffraction (XRD) (Bruker D8 ADVANCE system with Cu Kα of 1.5406 Å). Raman and photoluminescence (PL) spectra were recorded at room temperature by a Jobin Yvon LabRAM HR 800UV micro-Raman/PL system under an Ar^+ (514.5 nm) and He–Cd (325.0 nm) laser excitation, respectively.

3. Results and discussion

The Zn nanowires with little oxidation were synthesized at step one by thermal evaporation methods. Fig. 1(a) shows the XRD spectrum of one-step-prepared sample. Apart from strong Zn (0 0 2), (1 0 0), (1 0 1), and (1 0 2) diffraction peaks, there are also very weak ZnO (1 0 0), (0 0 2), and (1 0 1) peaks [17], which indicates that the

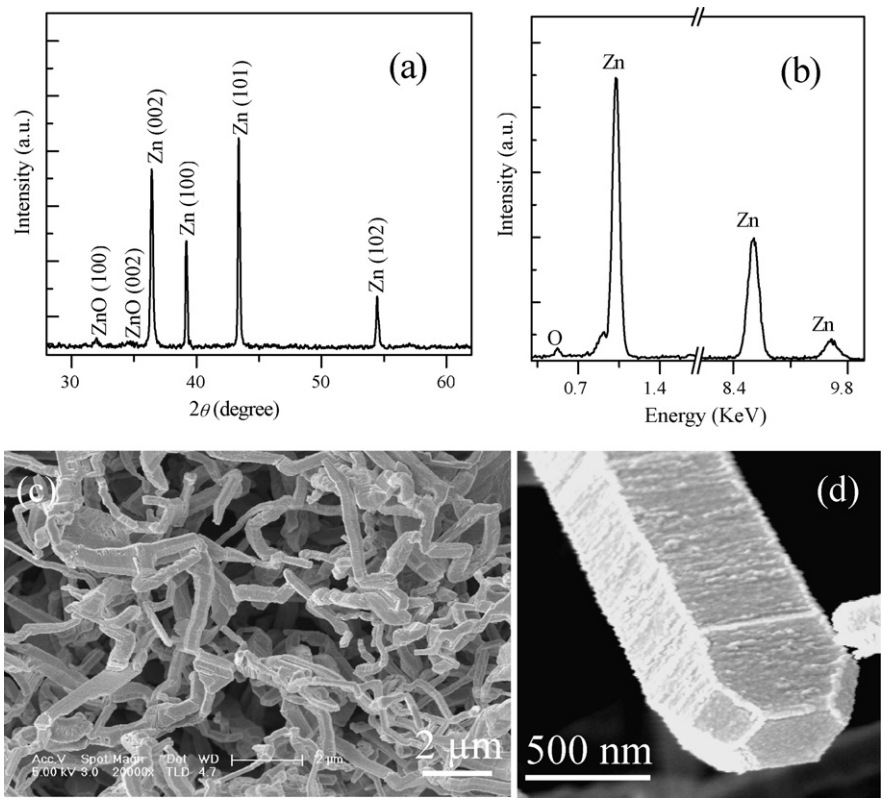

Fig. 1. (a) XRD spectrum of the one-step-prepared product. (b) EDX spectrum of the corresponding sample. (c) Low- and (d) high-magnification SEM images of hexagonal-shaped nanowires.

prepared samples at step one is mainly composed of a great number of Zn with little oxidation. Furthermore, it also implies that during the growth process, no other metal was used as the catalyst or additive. The energy dispersive X-ray (EDX) spectrum in Fig. 1(b) further confirms the above-mentioned arguments. The relative large atomic ratio of Zn and O (∼19:1) also indicates that little Zn is oxidized at the first step due to the low substrate temperature. Fig. 1(c) shows the FESEM image of the one-step-prepared samples, which exhibits the general morphology of nanowires with 300–600 nm widths and length up to several-decade microns. Fig. 1(d) displays the high-magnification image of single nanowire.

As shown in Fig. 1(d), the hexagon-shaped mounds were observed at the end of nanowires without any nanoparticles, suggesting that the growth mechanism is not vapor–liquid–solid (VLS) process, since a typical characteristic of VLS is the existence of nanoclusters capping at the end of a 1D nanostructure [23,24]. The layered structures on the side-wall suggest that the nanowires are grown by the layer-by-layer growth mechanism. The mound-like morphology strongly implies that the existence of an Ehrlich–Schwoebel barrier (ESB) during the formation of nanowires [13]. The ESB is an energy barrier for adspecies to jump from a higher terrace to lower one at the edge of step. Due to the existence of such barrier, the next atomic layer may nucleate before the previous layer is completed, which generally results in the multilayer structure and the appearance of mounds [13,25]. During the synthesis of nanowires, a number of Zn and ZnO_x ($x \leq 1$) molecules or clusters and relatively high temperature are helpful to overcome the influence of barrier and make particle diffuse over crystalline surface step stage, which can lead to the layer-by-layer growth of nanowires. However, when the samples were cooled down, the ESB plays an important role in the formation of the mound-like nanotop. Similar observation has been reported by Liu et al. [13]. In Fig. 1(d), the layered side-wall and mound-like nanotop clearly demonstrate the above argument concerning the formation mechanism of nanowires.

According to the above experimental observations, we can deduce the growth process as follow: In the initial stage of heating Zn powder, Zn vapor with little Zn oxidized into ZnO_x ($x \leq 1$) molecules or clusters is formed due to the

limited oxygen content. Zn and its oxide are transported to the low-temperature region by the carrier gas and absorbed on the surface of Si substrate. Since Zn belongs to the hexagonal crystal system with the sixfold symmetry, Zn and ZnO_x molecules or clusters on the substrate could migrate to form the steady hexagonal nanostructure, and then the nanowires can grow with the continuous supplementation of Zn and ZnO_x. Owing to the introduction of oxygen, the surface of nanowires could be oxidized into ZnO during the growth process of nanowires. Even when the samples are naturally cooled, their surface may be still oxidized. However, it should be noticed that the nanowires could not be completely oxidized into ZnO because of the low substrate temperature (only ~200 °C). As shown in the XRD pattern of Fig. 1(a), the simultaneous appearance of Zn and ZnO diffraction peaks confirms our arguments as well.

The XRD analysis and EDX spectrum were employed to determine the structure and component of the prepared products at step two, which were made by heating the one-step-prepared samples and evaporating simultaneously the Zn powder. Fig. 2(a) displays the XRD pattern of samples prepared at the second step. All the peaks reveal the typical wurtzite hexagonal phase of ZnO [26]. Apart from the ZnO diffraction peaks, no other peaks, such as Zn peaks, are detected, indicating that the prepared products at step two are wurtzite ZnO. Compared with EDX spectrum of the step-one samples (Fig. 1(b)), the atomic ratio of Zn and O decreases to 1.03:1 in Fig. 2(b), which further confirms that the one-step-prepared products are completely oxidized into ZnO at step two due to the high substrate temperature.

The morphology and structure of the prepared products at step two were analyzed by SEM. Fig. 2(c) shows the SEM image of samples fabricated at step two, displaying an interesting hierarchical pure ZnO nanostructure with lengths of several decade microns. The high-magnification images of single ZnO nanostructure in Fig. 2(d) and (e) reveal that they are composed of central axial nanowires surrounded by radially oriented nanorods with 6-fold structural symmetry. Fig. 2(f) shows the side-wall image of hierarchical ZnO nanostructure with widths of 70–120 nm and average length of around 600 nm. The high-magnification image of the single nanorod on the side-wall displays columniform structure with a conic tip which is quite different from the hexagonal structure in Fig. 1(d), indicating that the ZnO nanorods are not synthesized through the layer-by-layer growth model. It is noticed that under the bottom of nanorods, ZnO layer with the 60° angle between the nearest neighbors is formed on the side-wall of central axial nanowires, as shown with white arrow in Fig. 2(e) and (f); Meanwhile, the large nanoclusters are found existing on the bottom of nanorods, as shown with black arrows in Fig. 2(f). These observations imply the following formation process of nanorods: At the initial stage of heating, the ZnO layer is first formed on the surface of nanowires. And then

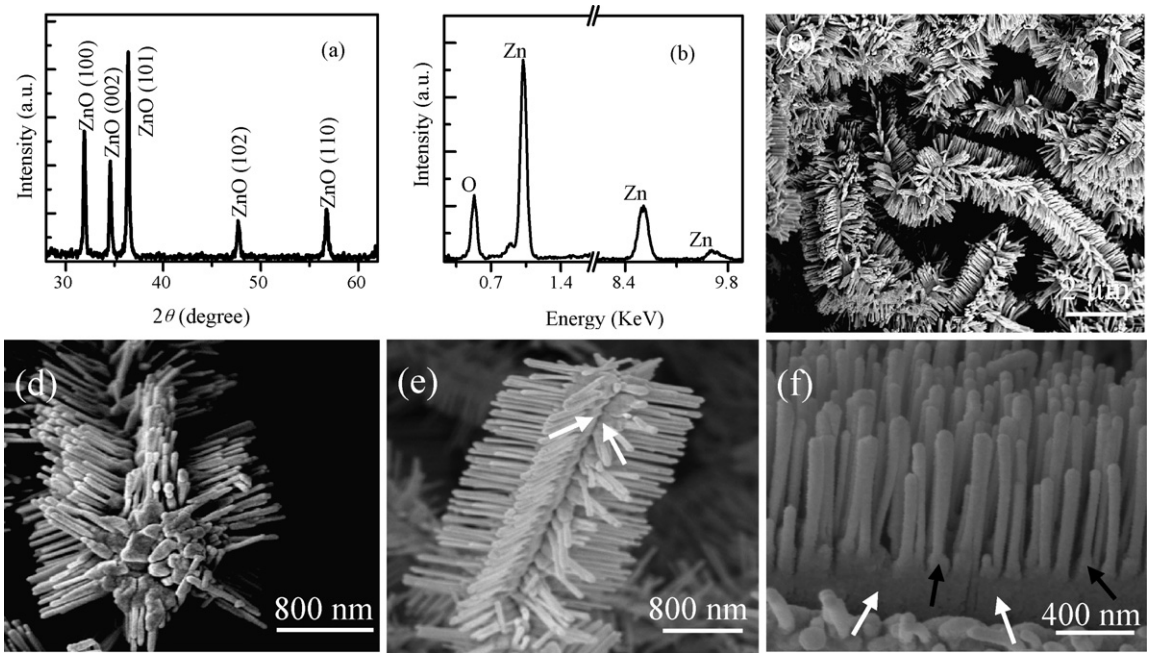

Fig. 2. (a) XRD spectrum of the prepared sample at step two, (b) EDX spectrum of the corresponding sample, (c) low magnification SEM image of the two-step-prepared product, (d) and (e) high-magnification SEM image of single hierarchical pure ZnO nanostructure, (f) SEM image of nanorods on the side-wall of central axial nanowire.

with the continuous supplementation of Zn and ZnO_x, they nucleate on the surface of ZnO layer and form the large nanoclusters. With the further absorption, ZnO nanorods grow from the top of nanoclusters.

The detailed structure of individual hierarchical ZnO nanostructure can be characterized by the HRTEM and SAED. The TEM morphology in Fig. 3(a) also clearly displays that single ZnO nanostructure is composed of central axial nanowires and radially oriented nanorods, which further confirms the SEM observation. Fig. 3(b) reveals the high-magnification image of side-wall. It can be observed that there are no nanoclusters forming on the tip of nanorods. Fig. 3(c) displays the HRTEM image of nanorod (indicated by the ellipse in Fig. 3(b)). The lattice fringes of ZnO nanorod indicate that nanorod is single crystalline with a uniform structure and no noticeable stacking faults. However, there is the blurry region (indicated by the ellipse in Fig. 3(c)), implying the probable existence of other deficiencies. The lattice spacing of 0.28 nm corresponds to the spacing of [1 0 0] crystal planes of wurtzite ZnO. The SAED pattern of corresponding nanorod, as shown in the inset of Fig. 3(c), further demonstrates the formation of high-quality single crystalline nanorods on the nanowire's surface. It is noticed that the growth orientation of nanorods are not along the preferential growth direction in the *c*-axis [0 0 0 1], but along [$1\bar{2}14$] one. To clearly reveal the reason of non-preferential growth, Fig. 3(d) displays the SAED pattern of central axial nanowire (the rectangle region in the inset of Fig. 3(b)), where the diffraction pattern of nanowire is similar to that of nanorod, indicating the epitaxial growth of nanorod from the side facet of nanowire. Considering this fact, we assume that the reason for no preferential growth of single nanorods should be attributed to the epitaxial relation between the central axial nanowire and nanorods on the side-wall. The similar experimental observation had been reported by Fan et al. [27] before.

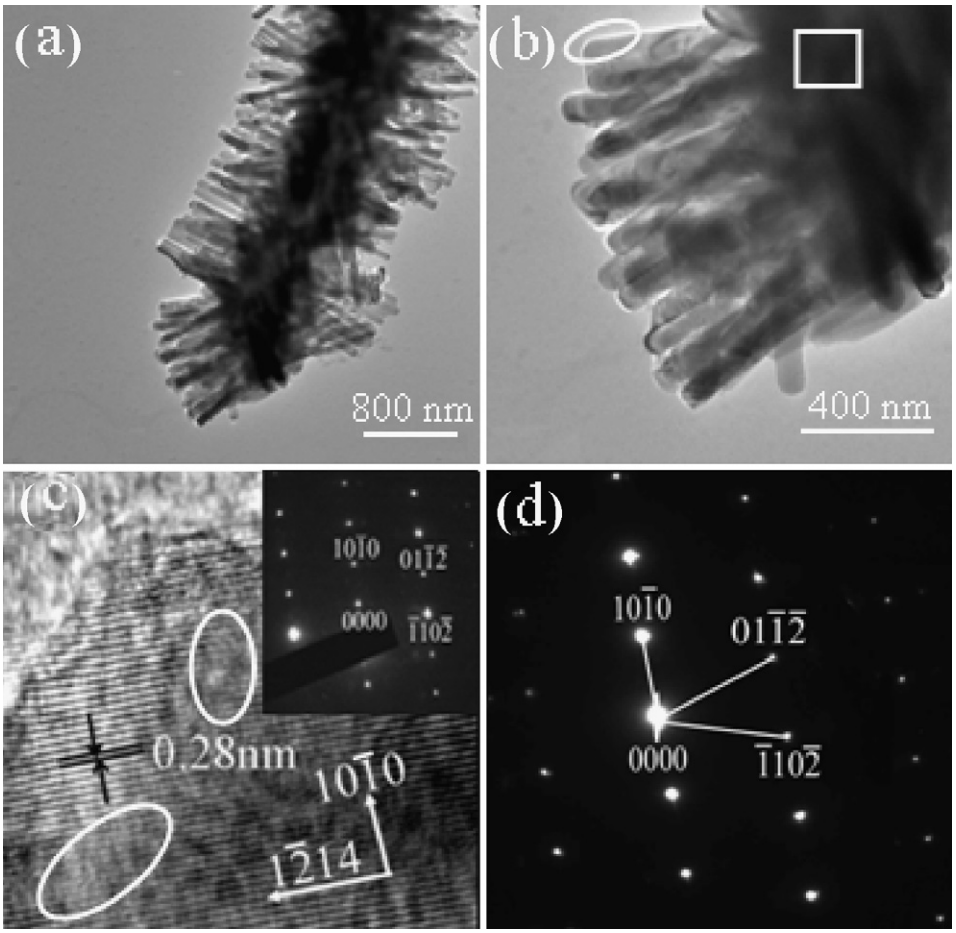

Fig. 3. (a) TEM and HRTEM images of single hierarchical pure ZnO nanostructure. (b) TEM image of nanorods on the side-wall of nanowire. (c) HRTEM image of a nanorod's tip indicated by the ellipse in (b), and (inset) SAED pattern of the corresponding nanorod. (d) SAED pattern of central axial nanowire indicated by the rectangle in (b).

The VLS mechanism cannot explain the growth mechanism of well-ordered nanorods; however, some literature precedent for the screw dislocation mechanism would be helpful. From the SEM and TEM images of Figs. 2(f) and 3(b), there are no additional metal particles appearing on the top of the nanorods, eliminating the catalysis-assisted VLS mechanism [21,24]. In the screw dislocation model, the growth rate along the dislocation line is much faster than that of the radius direction, resulting in the formation of crystal 1D nanostructure. And the conic tip at the end of 1D structured is the evidence for the 1D material growth via the screw dislocation mechanism [28,29]. From the SEM and TEM images in Figs. 2 and 3, the characteristics of smooth facets and rough tips without hexagonal shape also suggest the growth via the screw dislocation mechanism.

According to the above arguments, we can deduce the formation process of hierarchical pure ZnO nanostructure as follow: Zn and ZnO_x ($x \leq 1$) gases yielded by heating Zn powder at 500 °C are transported to the one-step-prepared nanowire substrate, leading to the deposition of ZnO layer on the surface of nanowires. The continuously supplied Zn and ZnO_x molecules or clusters nucleate on their surfaces forming the large nanoclusters. ZnO nanorods epitaxially grow from the surface of the nanowires through the screw dislocation mechanism due to the further absorption of nanocluster's tip on Zn and ZnO_x. In our experiment, we also observe that the nanorods are only formed on the side facet, not on the two ends of central axial nanowires, which is probably related to the relatively higher surface energy and coarse degree on the side facet. Furthermore, the different nucleation dimensions on the side-wall of central axial nanowires may contribute to the observed nonuniform width of nanorods. In addition, it should be mentioned that if the substrate was placed in front of Zn powder at the second step, ZnO nanotube can be prepared due to the absence of Zn source.

The optical properties of hierarchical pure ZnO nanostructure have been studied by room-temperature Raman and PL measurements. Fig. 4 displays Raman spectra of the as-prepared samples at step two and the annealed ones in the pure oxygen atmosphere. In an ideal ZnO crystal, only the optical phonons at the center of the Brillouin zone are involved in the first order Raman spectra. As for the nanomaterials, however, the phonons near the zone center must be considered, because the phonon scattering will not be limited to the center of Brillouin zone due to the relaxed momentum selection rule [30]. According to the group theory, near the Brillouin zone, only A_1, E_1, and $2E_2$ are Raman active in the eight different optic modes [31]. As shown in Fig. 4, besides the photon modes of silicon at ~518 cm^{-1}, there are three apparent ZnO photon modes appearing at 381, 437, and 581 cm^{-1}, which has been assigned to the A_1 (TO), E_2 (high), and E_1 (LO), respectively [30]. Compared with the Raman spectra of as-deposited samples, the increase of A_1 (TO) and E_2 (high) modes intensity implies the better crystal quality at the annealed samples [32]. It is generally accepted that E_1 (LO) mode is associated with the oxygen vacancies [33]. The decrease of E_1 (LO) intensity in annealing samples indicates that the annealing can be helpful to decrease the deficiency.

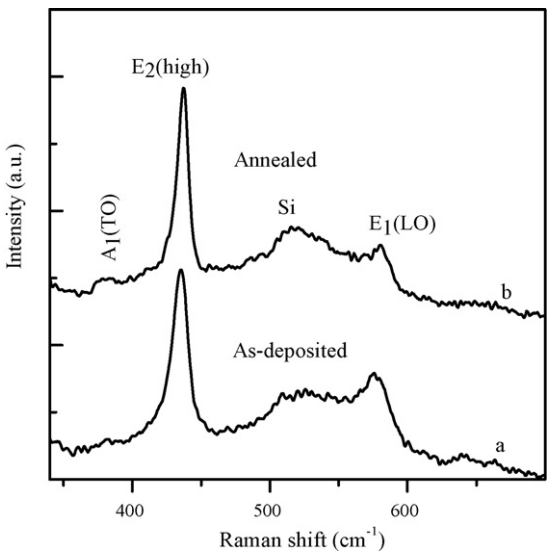

Fig. 4. Raman of the hierarchical ZnO nanostructures: (a) as-deposited samples; (b) annealed samples under oxygen atmosphere at 600 °C for 1 h.

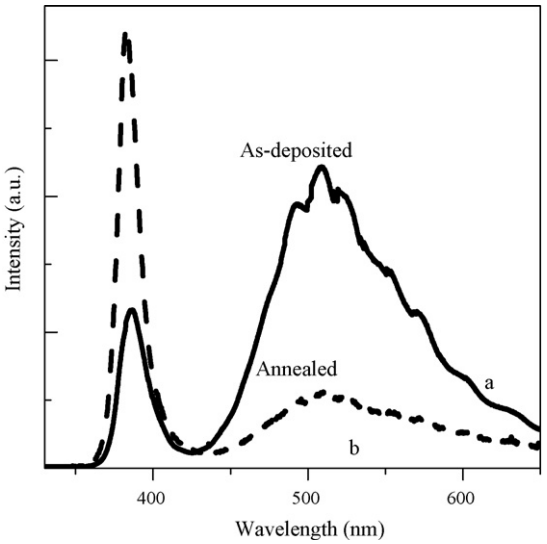

Fig. 5. PL spectra of the hierarchical ZnO nanostructures: (a) as-deposited samples; (b) annealed samples under oxygen atmosphere at 600 °C for 1 h.

PL emission is one of the most important properties for the novel nanostructures as we synthesized. For the as-deposited samples, there is a weak ultraviolet (UV) peak at ∼387 nm and a strong green emission at ∼511 nm, as shown in the solid curve of Fig. 5. It is generally accepted that, for ZnO film, the UV peak originates from the recombination of free exciton, and the green emission is related to the singly ionized oxygen vacancies [34]. To further investigate the luminescence mechanism of hierarchical ZnO nanostructures, we also display PL spectrum of the annealed samples in the pure oxygen atmosphere, as shown in the dashed curve of Fig. 5. It can be observed that after annealing, the intensity of UV peak greatly increases, but that of green peak decreases. Considering the fact that the annihilation of exciton will lead to the decrease of UV peak intensity for the samples of poor crystal quality [35], the increase of UV peak intensity for annealing samples implies that UV emission in the hierarchical ZnO nanostructures should originate from the exciton recombination of near-band-edge emission. Compared with the as-deposited samples, the annealing samples show decreases in both the intensity of green emission and the oxygen vacancies, indicating that the green peak should also be related to the oxygen vacancies. In addition, the strong green peak at the as-deposited samples also indicates that high surface-to-volume ratio is an important factor to affect the intensity of green emission as well. Yao et al. [36] also reported that the surface-to-volume ratio can influence significantly the PL emission efficiency.

4. Conclusions

In summary, the hierarchical pure ZnO nanostructures with 6-fold structural symmetry were synthesized by two-step thermal evaporation process without any catalyst. Detailed structural analysis reveals that the one-step-prepared samples are fabricated via the layer-by-layer growth mechanism and composed of hexagonal-shaped nanowires with a great number of Zn and little oxidation. SEM and HRTEM images of the prepared hierarchical ZnO nanostructures at step two reveal that individual hierarchical ZnO nanostructures consist of central axial ZnO nanowire and radially oriented ZnO nanorods with 6-fold structural symmetries. The corresponding SAED analyses show that single crystal ZnO nanorods epitaxially grow from the side-wall of central axial ZnO nanowires through the screw dislocation growth mechanism. By comparison with Raman and PL spectra of the as-deposited samples and the annealed ones in the pure oxygen atmosphere, we can deduce that for hierarchical pure ZnO nanostructure, the UV peak at ∼387 nm is related to the free exciton recombination, and the strong green peak emission is due to the oxygen vacancies and high surface-to-volume ratio. The present achievements of hierarchical pure ZnO nanostructures may have potential applications in multichannel optoelectronic devices due to the large surface area and high integration degree.

Acknowledgements

This work was supported by the Natural Science Foundation of China (contract Nos. 10674094 and 10734020), National Major Basic Research Project of 2006CB921507, the Minister of Education of PCSIRT (contract No. IRT0524), and the Shanghai Municipal Commission of Science and Technology Project of 06JC14039.

References

[1] X.D. Bai, P.X. Gao, Z.L. Wang, E.G. Wang, Appl. Phys. Lett. 82 (2003) 4806.
[2] M.H. Huang, S. Mao, H. Feick, H. Yan, Y. Wu, H. Kind, E. Weber, R. Russo, P. Yang, Science 292 (2001) 1897.
[3] S. Liang, H. Sheng, Y. Liu, Z. Huo, Y. Lu, H. Shen, J. Cryst. Growth 225 (2001) 110.
[4] Y. Chen, D. Bagnall, T. Yao, Mater. Sci. Eng. B 75 (2000) 190.
[5] J.Y. Lee, Y.S. Choi, J.H. Kim, M.O. Park, S. Im, Thin Solid Films 403 (2002) 553.
[6] Q.H. Li, Q. Wang, Y.J. Chen, T.H. Wang, H.B. Jia, D.P. Yu, Appl. Phys. Lett. 85 (2004) 636.
[7] N. Saito, H. Haneda, T. Sekiguchi, N. Ohashi, L. Sakaguchi, K. Koumoto, Adv. Mater. 14 (2002) 418.
[8] Y. Lin, Z. Zhang, Z. Tang, F. Yuan, J. Li, Adv. Mater. Opt. Electron. 9 (1999) 205.
[9] M. Law, L.E. Greene, J.C. Johnson, R. Saykally, P. Yang, Nat. Mater. 4 (2005) 455.
[10] Z.W. Pan, Z.R. Dai, Z.L. Wang, Science 291 (2001) 1947.
[11] X.Y. Kong, Y. Ding, R.S. Yang, Z.L. Wang, Science 303 (2004) 1348.
[12] M.J. Zheng, L.D. Zhang, G.H. Li, W.Z. Shen, Chem. Phys. Lett. 363 (2002) 123.
[13] D.F. Liu, Y.J. Xiang, Z.X. Zhang, J.X. Wang, Y. Gao, L. Song, L.F. Liu, X.Y. Dou, X.W. Zhao, S.D. Luo, C.Y. Wang, W.Y. Zhou, G. Wang, S.S. Xie, Nanotechnology 16 (2005) 2665.
[14] J.Y. Lao, J.Y. Huang, D.Z. Wang, Z.F. Ren, Nano. Lett. 3 (2003) 235.
[15] P.X. Guo, Z.L. Wang, Appl. Phys. Lett. 84 (2003) 2883.
[16] J.Q. Hu, Y. Bando, Appl. Phys. Lett. 82 (2003) 1401.
[17] J.Q. Hu, Q. Li, X.M. Meng, C.S. Lee, S.T. Lee, Chem. Mater. 15 (2003) 305.
[18] G.Q. Ding, W.Z. Shen, M.J. Zheng, D.H. Fan, Appl. Phys. Lett. 88 (2006) 103106.
[19] X.P. Gao, Z.F. Zheng, H.Y. Zhu, G.L. Pan, J.L. Bao, F. Wu, D.Y. Song, Chem. Commun. (2004) 1428.
[20] A. Umar, S. Lee, Y.H. Im, Y.B. Hahn, Nanotechnology 16 (2005) 2462.
[21] J.Y. Lao, J.G. Wen, Z.F. Ren, Nano. Lett. 2 (2002) 1287.
[22] R.C. Wang, C.P. Liu, J.L. Huang, S.J. Chen, Appl. Phys. Lett. 86 (2005) 251104.
[23] R.S. Wagner, W.C. Ellis, Appl. Phys. Lett. 4 (1964) 89.
[24] G.Z. Shen, Y. Bando, B.D. Liu, D. Golberg, C.J. Lee, Adv. Funct. Mater. 16 (2006) 410.
[25] W.C. Elliott, P.F. Miceli, T. Tse, P.W. Stephens, Phys. Rev. B 54 (1996) 17938.
[26] F.Q. He, Y.P. Zhao, Appl. Phys. Lett. 88 (2006) 193113.
[27] H.J. Fan, R. Scholz, F.M. Kolb, M. Zacharias, Appl. Phys. Lett. 85 (2004) 4142.
[28] X.L. Zhang, Y.S. Kang, Inorg. Chem. 45 (2006) 4186.
[29] N.S. Ramgir, D.J. Late, A.B. Bhise, M.A. More, I.S. Mulla, D.S. Joag, K. Vijayamohanan, J. Phys. Chem. B 110 (2006) 18236.
[30] R.P. Wang, G. Xu, P. Jin, Phys. Rev. B 69 (2004) 113303.
[31] J.M. Calleja, M. Cardona, Phys. Rev. B 16 (1977) 3753.
[32] G.W. Cong, H.Y. Wei, P.F. Zhang, J.J. Peng, X.L. Liu, C.M. Jiao, W.G. Hu, Q.S. Zhu, Z.G. Wang, Appl. Phys. Lett. 87 (2005) 231903.
[33] H. Pan, J.Z. Luo, H. Sun, Y.P. Feng, C. Poh, J.Y. Jing, Nanotechnology 17 (2006) 2963.
[34] D.H. Fan, Z.Y. Ning, M.F. Jiang, Appl. Surf. Sci. 245 (2005) 414.
[35] H.Q. Li, Z.Y. Ning, S.H. Cheng, M.F. Jiang, Acta Phys. Sin. 53 (2004) 3.
[36] B.D. Yao, Y.F. Chan, N. Wang, Appl. Phys. Lett. 81 (2002) 757.